

Parallel Channel Estimator and Equalizer for Mobile OFDM Systems

Yongfeng Guan · Tao Xu · Rene van Leuken ·
Manyi Qian

Received: 25 January 2013 / Revised: 28 August 2013 / Published online: 30 October 2013
© Springer Science+Business Media New York 2013

Abstract Mobile OFDM refers to OFDM systems with fast moving transceivers, in contrast to traditional OFDM systems whose transceivers are stationary or have a low velocity. In this paper, we use the basis expansion model (BEM) to model time-varying OFDM channels. Using different BEM's, we investigate various architectures to implement the least-squares (LS) channel estimation and its corresponding zero-forcing (ZF) channel equalization. The experimental results show that our implementation for mobile OFDM systems is capable of combatting the time variation of mobile OFDM channels, and more hardware resource utilization is necessary compared with a traditional OFDM design which fails in a time-varying scenario. For mobile OFDM systems, different BEM's are available for the channel modeling. We observe that the so-called Critically sampled Complex-Exponential BEM (CCE-BEM) leads to the most efficient hardware architecture while still maintaining high modeling accuracy.

Keywords OFDM · Time-varying channels · BEM

Y. Guan · T. Xu (✉)

National University of Defense Technology, Changsha, 410073, China
e-mail: xutao_2001640@nudt.edu.cn

Y. Guan

e-mail: guanyongfeng@nudt.edu.cn

T. Xu · R. van Leuken

Delft University of Technology, Delft, 2628CD, The Netherlands

R. van Leuken

e-mail: t.g.r.m.vanleuken@tudelft.nl

M. Qian

Beijing Jiaotong University, Beijing, 100044, China
e-mail: myqian@bjtu.edu.cn

1 Introduction

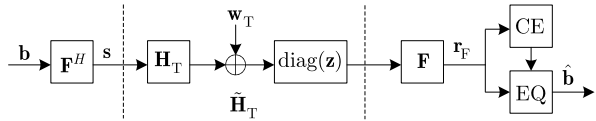
Future communication systems are required to support a high data transfer rate between fast moving terminals, e.g., vehicular communications. Orthogonal frequency division multiplexing (OFDM), as a bandwidth efficient multi-carrier transmission technique, shows attractive features to wireless radio applications [1]. It is well known that OFDM relies on the assumption that the channel stays constant within at least one OFDM symbol period to maintain the orthogonality among OFDM subcarriers. When temporal channel variation emerges due to the Doppler effect, this orthogonality is corrupted and non-negligible inter-carrier interference (ICI) is induced [3], severely deteriorating the system performance. In this case, channel equalization is necessary, for which we need accurate models of narrowband time-varying channels. It is common to describe the channel taps statistically by their Doppler spectrum which may be bathtub-shaped [12]. Despite their accuracy, these models are generally cumbersome. Hence, many works resort to a parsimonious channel modeling approach such as the basis expansion model (BEM) [8] to describe the channel dynamics. The optimal BEM in terms of the mean square error (MSE) is the discrete Karhuen–Loève BEM (DKL-BEM) [25] which, however, requires the true channel statistics and thus is not always practical. The discrete prolate spheroidal BEM (DPS-BEM) [27] is derived based on the channel statistics approximated by a rectangular spectrum. Avoiding the dependence on the channel statistics, the critically sampled complex-exponential BEM (CCE-BEM) [8] is proposed using complex exponentials as its basis functions. Due to its algebraic ease, the CCE-BEM is widely adopted, e.g. in [6–8, 13–17]. Additionally, the polynomial BEM (POL-BEM), which models each tap as a linear combination of a set of polynomials, has also gained attention for low Doppler spreads, e.g., in [2, 24]. The detailed comparison of the aforementioned BEMs can be found in [21, 27].

Research on OFDM systems from the aspect of the hardware implementations can also be found, e.g., on FPGA platforms [4] or using a specific digital signal processor (DSP) [20]. A complication of these works is assuming a time-invariant channel where the transceiver and significant scatterers are stationary or have a negligible velocity. Hence, the adopted OFDM systems are free of inter-carrier interference (ICI), and called “traditional OFDM” or time-invariant OFDM in this paper. To our knowledge, little attention has been paid to an efficient hardware implementation of mobile OFDM, which refers to the OFDM systems over rapidly time-varying channels. In this paper, we shall investigate efficient architectures corresponding to different BEM’s to implement the channel estimator and channel equalizer for mobile OFDM in the narrowband regime. Moreover, we then identify a particular model, among available BEM’s, which leads to the most efficient hardware architecture while still maintaining high modeling accuracy.

2 OFDM System Model in Light of BEM

Let us consider an OFDM system with N subcarriers as illustrated by Fig. 1. An OFDM symbol $\mathbf{b} = [b_0, b_1, \dots, b_{N-1}]^T$ is used to modulate N carriers as $\mathbf{s} = \mathbf{F}^H \mathbf{b}$,

Fig. 1 Transceiver block diagram



where \mathbf{F} stands for the N point unitary discrete Fourier transform (DFT) matrix with $[\mathbf{F}]_{m,k} = \frac{1}{\sqrt{N}}e^{-j2\pi \frac{mk}{N}}$. Subsequently, \mathbf{s} is concatenated by a cyclic prefix, sent over the channel, stripped from the cyclic prefix, reshaped by a windowing filter and converted into the frequency domain. When the cyclic prefix has a sufficient length to eliminate the inter-symbol interference between successive OFDM symbols [26], Fig. 1 illustrates the data flow of OFDM transmission by abstracting the cyclic prefix. Specifically, the OFDM system can be characterized as

$$\begin{aligned} \mathbf{r}_F &= \mathbf{FZ}\mathbf{H}_T\mathbf{F}^H\mathbf{b} + \mathbf{FZ}\mathbf{w}_T \\ &= \mathbf{F}\tilde{\mathbf{H}}_T\mathbf{F}^H\mathbf{b} + \mathbf{FZ}\mathbf{w}_T \\ &= \mathbf{H}_F\mathbf{b} + \mathbf{n}_F, \end{aligned} \tag{1}$$

where \mathbf{r}_F is the received sample vector in the frequency domain, $\mathbf{Z} = \text{diag}\{\mathbf{z}\}$ with $\mathbf{z} = [z_0, z_1, \dots, z_{N-1}]^T$ representing the time-domain windowing, while \mathbf{H}_T and $\tilde{\mathbf{H}}_T = \mathbf{Z}\mathbf{H}_T$ represents the channel matrix in the time domain without and with windowing, respectively. With $h_l^{(n)}$ denoting the l th channel tap at the n th time instant for $l = \{0, 1, \dots, L\}$ with L finite (i.e., $h_l^{(n)} = 0$ for $l < 0$ or $l > L$), we can specify \mathbf{H}_T as a ‘‘pseudo-circulant’’ matrix given by $[\mathbf{H}_T]_{k,m} = h_{(k-m)_{\text{mod}/N}}^{(m)}$, or

$$\mathbf{H}_T = \begin{bmatrix} h_0^{(0)} & & & h_L^{(0)} & \dots & h_1^{(0)} \\ \vdots & \ddots & & & \ddots & \vdots \\ h_L^{(L)} & \ddots & \ddots & \mathbf{0} & & h_L^{(L-1)} \\ & \ddots & \ddots & \ddots & \ddots & \\ \mathbf{0} & & \ddots & \ddots & \ddots & \\ & & & h_L^{(N-1)} & \dots & h_0^{(N-1)} \end{bmatrix}.$$

Obviously, $\tilde{\mathbf{H}}_T$ has the same structure as \mathbf{H}_T , but is composed by $\tilde{h}_l^{(n)} = z_n h_l^{(n)}$. Additionally, $\mathbf{n}_F = \mathbf{FZ}\mathbf{w}_T$ is the windowed frequency-domain noise, and $\mathbf{H}_F = \mathbf{F}\tilde{\mathbf{H}}_T\mathbf{F}^H$ is the effective frequency-domain channel matrix. We underscore that the time-domain windowing is normally not included in traditional OFDM systems, i.e., $\mathbf{Z} = \mathbf{I}_N$, however, it is required by mobile OFDM to suppress the ICI [17, 18]. Moreover, for traditional OFDM where the channel is time-invariant, $\tilde{\mathbf{H}}_T = \mathbf{H}_T$ is a circulant matrix since $h_l^{(n)} \equiv h_l^{(n')}$ for any $n \neq n'$, and thus \mathbf{H}_F is diagonal, while for mobile OFDM in the present of temporal channel changes, \mathbf{H}_F is a full matrix.

Stacking all the channel taps into a single vector $\tilde{\mathbf{h}} = [\tilde{\mathbf{h}}_0^T, \dots, \tilde{\mathbf{h}}_{N-1}^T]^T$ with $\tilde{\mathbf{h}}_n = [\tilde{h}_0^{(n)}, \tilde{h}_1^{(n)}, \dots, \tilde{h}_L^{(n)}]^T$, we use the BEM to model the channel [8, 21], regardless of

the modeling error, as

$$\tilde{\mathbf{h}} = (\mathbf{Q} \otimes \mathbf{I}_{L+1})\mathbf{c}, \tag{2}$$

where $\mathbf{c} = [\mathbf{c}_{-Q}^T, \dots, \mathbf{c}_Q^T]^T$ with $\mathbf{c}_q = [c_{q,0}, c_{q,1}, \dots, c_{q,L}]^T$ being the q th BEM coefficient vector corresponding to the q th basis expansion function \mathbf{q}_q , and $\mathbf{Q} = [\mathbf{q}_{-Q}, \dots, \mathbf{q}_Q]$ with $(2Q + 1)$ being the BEM order. (2) indicates that after introducing the BEM, one can estimate the BEM coefficients to perform channel estimation.

To this end, we can describe OFDM systems in light of BEM by substituting (2) into (1) as

$$\begin{aligned} \mathbf{r}_F &= \mathbf{F}\tilde{\mathbf{H}}_T\mathbf{F}^H\mathbf{b} + \mathbf{n}_F \\ &= \mathbf{F}\left(\sum_{q=-Q}^Q \text{diag}\{\mathbf{q}_q\}\mathbf{C}_q\right)\mathbf{F}^H\mathbf{b} + \hat{\mathbf{n}}_F \\ &= \sum_{q=-Q}^Q (\mathbf{F}\text{diag}\{\mathbf{q}_q\}\mathbf{F}^H)(\mathbf{F}\mathbf{C}_q\mathbf{F}^H)\mathbf{b} + \hat{\mathbf{n}}_F \\ &= \sum_{q=-Q}^Q \mathbf{D}_q\Delta_q\mathbf{b} + \hat{\mathbf{n}}_F \end{aligned} \tag{3}$$

$$= \hat{\mathbf{H}}_F\mathbf{b} + \hat{\mathbf{n}}_F, \tag{4}$$

where

$$\hat{\mathbf{H}}_F = \sum_{q=-Q}^Q \mathbf{D}_q\Delta_q \tag{5}$$

is the modeled channel matrix as the estimate of \mathbf{H}_F , $\hat{\mathbf{n}}_F$ combines \mathbf{n}_F and the BEM modeling error, \mathbf{C}_q is an $N \times N$ circulant matrix (assuming that $N > L$ which is usually the case) given by

$$\mathbf{C}_q = \begin{bmatrix} c_{q,0} & & & c_{q,L} & \cdots & c_{q,1} \\ \vdots & \ddots & & & & \vdots \\ c_{q,L} & \ddots & \ddots & \mathbf{0} & & c_{q,L} \\ & \ddots & \ddots & \ddots & & \\ & \mathbf{0} & \ddots & \ddots & \ddots & \\ & & & c_{q,L} & \cdots & c_{q,0} \end{bmatrix},$$

while

$$\mathbf{D}_q = \mathbf{F}\text{diag}\{\mathbf{q}_q\}\mathbf{F}^H \tag{6}$$

is a circulant matrix and $\Delta_q = \mathbf{F}\mathbf{C}_q\mathbf{F}^H$. Due to the circulant structure of \mathbf{C}_q , Δ_q can also be expressed as a diagonal matrix by

$$\Delta_q = \text{diag}\{\mathbf{F}^{(L)}\mathbf{c}_q\} \quad (7)$$

with $\mathbf{F}^{(L)}$ representing the first $L + 1$ columns of the Fourier matrix $\sqrt{N}\mathbf{F}$.

3 Algorithm Background Overview

We underline that there has been extensive research on the channel estimation and channel equalization for OFDM systems over narrowband linear time-varying (LTV) channels, e.g., for channel estimation in [6, 21, 24] and for channel equalization in [6, 7, 10, 16, 17, 23]. In this paper, we do not attempt to summarize these efforts, but instead focus on the least-squares (LS) channel estimation and zero-forcing (ZF) equalization for narrowband OFDM LTV channels. In the following, we first clarify the arrangement of all OFDM subcarriers, and then describe the detailed descriptions for channel estimation and equalization, respectively.

3.1 OFDM Carrier Arrangement

For time-varying OFDM systems, comb-type pilot subcarriers and guarded null subcarriers are usually required [15, 21]. Specifically, we assume that the N subcarriers of the OFDM symbol include N_P pilot subcarriers and $(N - N_D - N_P)$ null subcarriers, and thus, out of N carriers, only N_D subcarriers carry information which are called data subcarriers. Let us specify an OFDM symbol vector $\mathbf{b} = [b_0, b_1, \dots, b_{N-1}]^T$ which includes a pilot symbol set $\mathbf{b}^{(p)} = [b_0^{(p)}, \dots, b_{N_P-1}^{(p)}]^T$, and a data symbol set $\mathbf{b}^{(d)} = [b_0^{(d)}, \dots, b_{N_D-1}^{(d)}]^T$ as well as zeros at null subcarriers. At the receiver, according to (4), the noiseless received sample vector is modeled by $\mathbf{r}_F = \hat{\mathbf{H}}_F\mathbf{b}$, where $\hat{\mathbf{H}}_F$ is (approximately) a banded matrix with a bandwidth of $2Q + 1$. Illustratively, as depicted in Fig. 2. between \mathbf{b} and \mathbf{r}_F , the banded channel matrix $\hat{\mathbf{H}}_F$ is placed whose bandwidth is $2Q + 1$. Moreover, the gray part of $\hat{\mathbf{H}}_F$ in Fig. 2 stands for significant non-zero entries, while its blank part represents the trivial entries (which will be zeros if the CCE-BEM is used).

In order to combat a narrowband time-varying OFDM channel modeled by $\hat{\mathbf{H}}_F$, it is crucial to carefully allocate these subcarriers and their corresponding observations [15, 21]. We follow [21] to arrange OFDM subcarriers. These N_P pilots are distributed into the OFDM symbol, and every transmitted pilot is guarded by $2Q$ null subcarriers to diminish mutual influences with adjacent data subcarriers in the present of Doppler frequency shifts. The rest of null subcarriers are placed on edge positions, and we require that the number of edge null subcarriers is sufficiently large (i.e., $\geq Q$) [6, 7, 16, 17], whose reason will be evident later on. In such a manner, the N_D data subcarriers are separated into several isolated clusters. If we assume that each data subcarrier cluster has the same length B for simplicity reasons, the m th isolated transmitted data subcarrier cluster is denoted by a $B \times 1$ vector $\mathbf{b}_m^{(d)} = [b_0^{(d,m)}, \dots, b_{B-1}^{(d,m)}]^T \subset \mathbf{b}^{(d)}$, for $m \in \{0, 1, \dots, N_B - 1\}$ with

$$N_B = N_D/B.$$

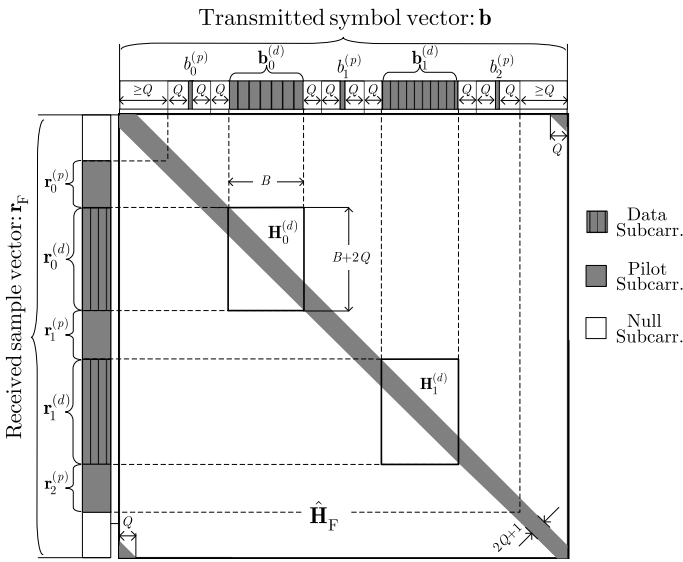


Fig. 2 OFDM subcarrier allocation illustration

Illustratively, such an arrangement of the OFDM subcarriers is depicted in Fig. 2, with $N_P = 3$. From there, it is clear that within the transmitted OFDM symbol \mathbf{b} , the guarded pilots $b_k^{(p)}$ and null edge subcarriers separate the N_D data subcarriers into $N_P - 1$ clusters.

At the receiver, corresponding to this m th transmitted data cluster $\mathbf{b}^{(d,m)}$, we build an observation window denoted by a $(B + 2Q) \times 1$ vector $\mathbf{r}_m^{(d)} = [r_{-Q}^{(d,m)}, \dots, r_0^{(d,m)}, \dots, r_{B-1}^{(d,m)}, \dots, r_{B-1+Q}^{(d,m)}]^T \subset \mathbf{r}_F$. Likewise, corresponding to the k th transmitted pilot $b_k^{(p)}$, for $k \in \{0, 1, \dots, N_P - 1\}$, its observation window is denoted as a $(2Q + 1) \times 1$ vector $\mathbf{r}_k^{(p)} = [r_{-Q}^{(p,k)}, \dots, r_0^{(p,k)}, \dots, r_Q^{(p,k)}]^T \subset \mathbf{r}_F$. In Fig. 2, the locations of these observation windows is also illustrated. We note that other options for the observation window are available [21], but the method adopted here is the optimal choice for LS channel estimation [21].

3.2 LS Channel Estimation

Pilots and their observations at the receiver are used to estimate time-varying channels. We recall the $N_P \times 1$ vector $\mathbf{b}^{(p)} = [b_0^{(p)}, \dots, b_{N_P-1}^{(p)}]^T$ which stacks all pilot symbols, and let the $(2Q + 1)N_P \times 1$ vector $\mathbf{r}^{(p)} = [\mathbf{r}_0^{(p)T}, \dots, \mathbf{r}_{N_P-1}^{(p)T}]^T$ represent all the received samples within the pilot observation windows embedded in \mathbf{r}_F . Then from (3), we obtain

$$\mathbf{r}^{(p)} = \sum_{q=-Q}^Q \mathbf{D}_q^{(p)} \Delta_q^{(p)} \mathbf{b}^{(p)} + \hat{\mathbf{n}}^{(p)}, \tag{8}$$

where $\mathbf{D}_q^{(p)}$ is a submatrix obtained from \mathbf{D}_q by only selecting the rows (columns) corresponding to $\mathbf{r}^{(p)}$ in \mathbf{r}_F ($\mathbf{b}^{(p)}$ in \mathbf{b}); $\Delta_q^{(p)}$ is obtained from Δ_q by selecting the rows of $\mathbf{b}^{(p)}$ in \mathbf{b} , while $\hat{\mathbf{n}}^{(p)}$ not only contains the noise obtained from $\hat{\mathbf{n}}_F$ in a similar manner but also includes crosstalk components from different positions of the data subcarriers (see [21] for details). We note that in this paper the statistics of $\hat{\mathbf{n}}^{(p)}$ is irrelevant since we focus on an LS channel estimation.

In order to estimate the BEM coefficients in \mathbf{c} , we now convert (8) (see Appendix for the detailed derivations) into

$$\mathbf{r}^{(p)} = \mathbf{A}^{(p)} \mathbf{c} + \hat{\mathbf{n}}^{(p)}, \quad (9)$$

where the $(2Q+1)N_P \times (2Q+1)(L+1)$ matrix $\mathbf{A}^{(p)}$ is specified as

$$\mathbf{A}^{(p)} = \mathbf{D}^{(p)} (\mathbf{I}_{2Q+1} \otimes (\text{diag}\{\mathbf{b}^{(p)}\} \mathbf{F}^{(L,p)})) \quad (10)$$

and

$$\mathbf{D}^{(p)} = [\mathbf{D}_{-Q}^{(p)}, \dots, \mathbf{D}_Q^{(p)}],$$

while $\mathbf{F}^{(L,p)}$ collects the rows of $\mathbf{F}^{(L)}$ corresponding to the positions of $\mathbf{b}^{(p)}$ in \mathbf{b} . It is noteworthy that $\mathbf{A}^{(p)}$ is only related to the pilot symbols $\mathbf{b}^{(p)}$, the BEM basis functions \mathbf{q}_q 's [cf. (6)] and the normalized Fourier matrix \mathbf{F} , all of which are perfectly known at the receiver. In other words, $\mathbf{A}^{(p)}$ can be pre-computed when designing the channel estimator (CE).

Based on the LS criterion, we obtain the estimate of the BEM coefficient vector from (9) given by

$$\hat{\mathbf{c}} = (\mathbf{A}^{(p)H} \mathbf{A}^{(p)})^{-1} \mathbf{A}^{(p)H} \mathbf{r}^{(p)}, \quad (11)$$

which has less entries than the channel gain vector $\tilde{\mathbf{h}}$ [cf. (2)] when $N > (2Q+1)$ as usually the case. It also explains the benefit of introducing the BEM since it allows for reducing the number of the estimated parameters. If we rewrite

$$\hat{\mathbf{c}} = [\hat{\mathbf{c}}_{-Q}^T, \dots, \hat{\mathbf{c}}_Q^T]^T$$

it is clear that $\hat{\mathbf{c}}_q$ estimates the q th BEM coefficient vector \mathbf{c}_q . Here it is noteworthy that $N_P > L$ is assumed in this paper so that $\mathbf{A}^{(p)H} \mathbf{A}^{(p)}$ is invertible (otherwise, pilots from multiple OFDM symbols are needed to be jointly considered to perform the channel estimation [22], which is not included in this thesis).

However, the final purpose of the estimator is not these BEM coefficients, but the channel between the transmitted data subcarriers and their corresponding observations at the receiver [6, 7], e.g., $\mathbf{H}_m^{(d)}$ in Fig. 2. It shall be equalized by the channel equalizer (EQ) to recover the transmitted data symbols that carry information. As illustrated in Fig. 2, the data subcarriers and their observation windows are divided into isolated clusters. Instead of handling the whole OFDM symbol jointly, we can parallelize the estimation for each cluster. Specifically, we explicitly write the m th

observation vector $\mathbf{r}_m^{(d)}$ that corresponds to $\mathbf{b}_m^{(d)}$ for $m \in \{0, 1, \dots, N_B - 1\}$, regardless of noise, as

$$\begin{aligned} \mathbf{r}_m^{(d)} &= \sum_{q=-Q}^Q \mathbf{D}_{q,m}^{(d)} \Delta_{q,m}^{(d)} \mathbf{b}_m^{(d)} \\ &= \sum_{q=-Q}^Q \mathbf{D}_{q,m}^{(d)} \text{diag}(\mathbf{F}_m^{(L,d)} \mathbf{c}_q) \mathbf{b}_m^{(d)} \end{aligned} \tag{12}$$

$$= \mathbf{H}_m^{(d)} \mathbf{b}_m^{(d)}, \tag{13}$$

where $\mathbf{D}_{q,m}^{(d)}$ is a $(B + 2Q) \times B$ submatrix obtained from \mathbf{D}_q by selecting rows (columns) corresponding to $\mathbf{r}_m^{(d)}$ in \mathbf{r}_F ($\mathbf{b}_m^{(d)}$ in \mathbf{b}); $\mathbf{F}_m^{(L,d)}$ is obtained from $\mathbf{F}^{(L)}$ by selecting the rows of $\mathbf{b}_m^{(d)}$ in \mathbf{b} , and $\Delta_{q,m}^{(d)} = \text{diag}(\mathbf{F}_m^{(L,d)} \mathbf{c}_q)$ is obtained from Δ_q similarly, while the $(B + 2Q) \times B$ sub-channel matrix

$$\mathbf{H}_m^{(d)} = \sum_{q=-Q}^Q \mathbf{D}_{q,m}^{(d)} \text{diag}(\mathbf{F}_m^{(L,d)} \mathbf{c}_q). \tag{14}$$

By replacing \mathbf{c}_q in (14) with $\hat{\mathbf{c}}_q$ from (11), we obtain

$$\begin{aligned} \hat{\mathbf{H}}_m^{(d)} &= \sum_{q=-Q}^Q \mathbf{D}_{q,m}^{(d)} \text{diag}(\mathbf{F}_m^{(L,d)} \hat{\mathbf{c}}_q) \\ &= \sum_{q=-Q}^Q \hat{\mathbf{H}}_{q,m}^{(d)}, \end{aligned} \tag{15}$$

where $\hat{\mathbf{H}}_{q,m}^{(d)}$ is the q th component of $\hat{\mathbf{H}}_m^{(d)}$, which is specified as

$$\hat{\mathbf{H}}_{q,m}^{(d)} = \mathbf{D}_{q,m}^{(d)} \text{diag}(\mathbf{F}_m^{(L,d)} \hat{\mathbf{c}}_q).$$

3.3 ZF Channel Equalization

After obtaining each $\hat{\mathbf{H}}_m^{(d)}$, a ZF equalization is carried out accordingly given by

$$\hat{\mathbf{b}}_m^{(d)} = (\hat{\mathbf{H}}_m^{(d)H} \hat{\mathbf{H}}_m^{(d)})^{-1} \hat{\mathbf{H}}_m^{(d)H} \mathbf{r}_m^{(d)}, \tag{16}$$

where $\hat{\mathbf{b}}_m^{(d)}$ is a $B \times 1$ vector as an estimate of $\mathbf{b}_m^{(d)}$. We perform (16) for $m = \{0, 1, \dots, N_B\}$ and thus all the transmitted data symbols are recovered.

It is known that the inversion of a $B \times B$ matrix $\hat{\mathbf{H}}_m^{(d)H} \hat{\mathbf{H}}_m^{(d)}$ is costly when it is considered as a full matrix [9]. As mentioned before, $\hat{\mathbf{H}}_F$ is a banded matrix approximately (or exactly when the CCE-BEM is used) and the matrix bandwidth is $(2Q + 1)$ that is usually much less than the matrix size. Therefore, we are allowed to reduce the

computational complexity of inverting $\hat{\mathbf{H}}_m^{(d)H} \hat{\mathbf{H}}_m^{(d)}$, if the trivial entries (or zeros when the CCE-BEM is used) outside the matrix bandwidth are removed from $\hat{\mathbf{H}}_F$ (equiv. from $\hat{\mathbf{H}}_m^{(d)}$) [cf. Fig. 2]. Such operation is well motivated by the fact that the energy of these trivial entries is reasonably negligible, thus allowing for a significant reduction of the equalization complexity at the price of an acceptable performance loss [6, 7, 16–18]. We will discuss this in more detail in Sect. 4.2. Inspired by these works [6, 7, 16–18], we first introduce a $(B + 2Q) \times B$ selecting matrix which only has ones within a $2Q + 1$ bandwidth or zeros otherwise, as depicted by

$$\Theta = \begin{bmatrix} 1 & & \mathbf{0} \\ \vdots & \ddots & \\ 1 & \mathbf{1} & 1 \\ & \ddots & \vdots \\ \mathbf{0} & & 1 \end{bmatrix}.$$

Then, instead of $\hat{\mathbf{H}}_m^{(d)}$ defined in (15), we shall actually substitute into (16) its adapted version after removing trivial entries. Specifically, we adapt (15), by introducing Θ , as

$$\begin{aligned} \hat{\mathbf{H}}_m^{(d)} &= \Theta \odot \sum_{q=-Q}^Q \mathbf{D}_{q,m}^{(d)} \text{diag}(\mathbf{F}_m^{(L,d)} \hat{\mathbf{c}}_q) \\ &= \sum_{q=-Q}^Q (\Theta \odot \mathbf{D}_{q,m}^{(d)}) \text{diag}(\mathbf{F}_m^{(L,d)} \hat{\mathbf{c}}_q) \end{aligned} \tag{17}$$

$$= \sum_{q=-Q}^Q \hat{\mathbf{H}}_{q,m}^{(d)}, \tag{18}$$

where \odot stands for the Hadamard (element-wise) product, and

$$\hat{\mathbf{H}}_{q,m}^{(d)} = \Theta \odot \mathbf{D}_{q,m}^{(d)} \text{diag}(\mathbf{F}_m^{(L,d)} \hat{\mathbf{c}}_q).$$

Here, we note that we keep the same notations (i.e., $\hat{\mathbf{H}}_m^{(d)}$ and $\hat{\mathbf{H}}_{q,m}^{(d)}$) as in (15) for notation ease. To avoid any confusion, in the remainder of this paper, we will refer to (18) as the definition of $\hat{\mathbf{H}}_m^{(d)}$ unless explicitly defined.

4 Parallel Implementation Architecture

After reviewing the background of LS channel estimation and ZF equalization for narrowband OFDM time-varying channels, we shall in this section describe efficient architectures for their implementation.

4.1 Channel Estimator

As mentioned in Sect. 3.3, we understand that the channel estimator yields $\hat{\mathbf{H}}_m^{(d)}$'s as defined in (18), for $m \in \{0, 1, \dots, N_B - 1\}$, which shall be used by the channel equalizer in practice.

General LS estimator To efficiently implement the LS estimator, we first combine (11) and (17) to avoid the unnecessary computations on known matrices (i.e., $\mathbf{A}^{(p)}$ and $\mathbf{F}_m^{(L,d)}$'s).

Let us first introduce a $(2Q + 1)B \times (2Q + 1)N_P$ matrix

$$\mathbf{M}_m = (\mathbf{I}_{2Q+1} \otimes \mathbf{F}_m^{(L,d)}) (\mathbf{A}^{(p)H} \mathbf{A}^{(p)})^{-1} \mathbf{A}^{(p)H},$$

and then obtain a $B \times (2Q + 1)N_P$ submatrix $\mathbf{M}_{q,m}$ that is embedded in \mathbf{M}_m at the rows corresponding to $\hat{\mathbf{c}}_q$ in $\hat{\mathbf{c}}$ [cf. (11)]. In this way, we can obtain an equation [cf. (11)] given by

$$\mathbf{F}_m^{(L,d)} \hat{\mathbf{c}}_q = \mathbf{M}_{q,m} \mathbf{r}^{(p)}.$$

Now, we rewrite (17), for $m \in \{0, \dots, N_B - 1\}$, as

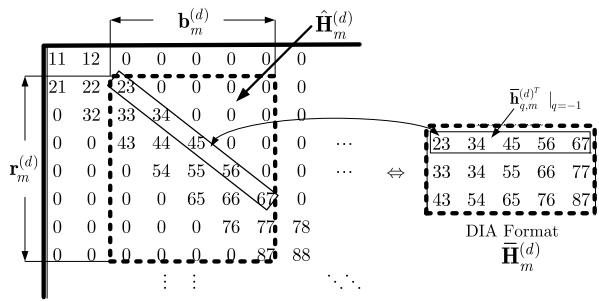
$$\begin{aligned} \hat{\mathbf{H}}_m^{(d)} &= \sum_{q=-Q}^Q (\Theta \odot \mathbf{D}_{q,m}^{(d)}) \text{diag}(\mathbf{F}_m^{(L,d)} \hat{\mathbf{c}}_q) \\ &= \sum_{q=-Q}^Q (\Theta \odot \mathbf{D}_{q,m}^{(d)}) \text{diag}(\mathbf{M}_{q,m} \mathbf{r}^{(p)}) \tag{19} \\ &= \sum_{q=-Q}^Q \hat{\mathbf{H}}_{q,m}^{(d)}, \tag{20} \end{aligned}$$

where we rewrite $\hat{\mathbf{H}}_{q,m}^{(d)}$ in (18) as $\hat{\mathbf{H}}_{q,m}^{(d)} = (\Theta \odot \mathbf{D}_{q,m}^{(d)}) \text{diag}(\mathbf{M}_{q,m} \mathbf{r}^{(p)})$.

Next, we reduce memory utilization by exploiting special matrix structures. We observe that $\Theta \odot \mathbf{D}_{q,m}^{(d)}$ is a banded Toeplitz matrix with a bandwidth of $(2Q + 1)$, which is obtained from the circulant matrix \mathbf{D}_q [cf. (6)] corresponding to the position of $\hat{\mathbf{H}}_m^{(d)}$ in $\hat{\mathbf{H}}_F$. It indicates that we only need the first $2Q + 1$ entries in the first column of this circulant matrix \mathbf{D}_q to represent all $\Theta \odot \mathbf{D}_{q,m}^{(d)}$'s for $m \in \{0, \dots, N_B - 1\}$. We denote a vector \mathbf{d}_q to stack these $2Q + 1$ entries. Moreover, $\hat{\mathbf{H}}_m^{(d)}$ is a banded matrix with a bandwidth of $(2Q + 1)$ [cf. (19)], and hence a memory efficient storage, called the DIA format [11], is adopted in this paper. Figure 3 illustrates how $\hat{\mathbf{H}}_m^{(d)}$ is represented by its DIA format $\tilde{\mathbf{H}}_m^{(d)}$, where $Q = 1$ is used and $\tilde{\mathbf{h}}_{q,m}^{(d)T}$ stands for the $(Q + q)$ th row in $\tilde{\mathbf{H}}_m^{(d)}$. Likewise, we denote $\tilde{\mathbf{H}}_{q,m}^{(d)}$ as the DIA format of $\hat{\mathbf{H}}_{q,m}^{(d)}$ in (20).

Finally, we describe the steps to efficiently implement (19) as Algorithm 1, which is suitable for any BEM model, and the only difference lies in the values of ROM components (i.e., $\mathbf{M}_{q,m}$'s and \mathbf{d}_q 's) when different BEM models are selected. Hence

Fig. 3 Efficient DIA storage for band matrices



Algorithm 1 General LS estimator

0. Pre-compute each matrix $\mathbf{M}_{q,m}$, for $q \in \{-Q, \dots, Q\}$ and $m \in \{0, \dots, N_B - 1\}$, and a single vector \mathbf{d}_q to present all $\Theta \odot \mathbf{D}_{q,m}^{(d)}$'s, for $q = \{-Q, \dots, Q\}$; Thus, totally $(N_P N_D + 1)(2Q + 1)^2$ complex elements are stored in ROM;
1. Perform (19) equivalently using \mathbf{d}_q and $\mathbf{M}_{q,m}$, by
 - (a) First calculating the $B \times 1$ vector $\mathbf{t}_{q,m} = \mathbf{M}_{q,m} \mathbf{r}^{(p)}$;
 - (b) Then scaling \mathbf{d}_q with each entry of $\mathbf{t}_{q,m}$ to attain each column of the $(2Q + 1) \times B$ matrix $\tilde{\mathbf{H}}_{q,m}^{(d)}$;
 - (c) Finally summing these $\tilde{\mathbf{H}}_{q,m}^{(d)}$'s for $q \in \{-Q, \dots, Q\}$ to yield $\tilde{\mathbf{H}}_m^{(d)}$, the DIA format of $\hat{\mathbf{H}}_m^{(d)}$.

Table 1 Computation complexity analysis for channel estimator

Complex operations	Estimator architecture	
	Simplified (for CCE-BEM)	General
CMs	$(2Q + 1)N_P B$	$(2Q + 1)(N_P + N_B)B$
CAs	$(2Q + 1)(N_P - 1)B$	$(2Q + 1)(2Q + N_P) - 1)B$

we call it “General LS estimator”. In this algorithm, we underscore that the m th channel estimator actually yields the DIA format $\tilde{\mathbf{H}}_m^{(d)}$ instead of its original $\hat{\mathbf{H}}_m^{(d)}$. The computational complexity of the implementation for the m th estimator using Algorithm 1 is specified in Table 1 which lists the number of required complex multipliers (CMs) and complex adders (CAs) for the m th estimator, for $m \in \{0, \dots, N_B - 1\}$. Its implementation schematic is depicted in Fig. 4. To maximize the processing concurrency, the parallelism for $m \in \{0, \dots, N_B - 1\}$ can be adopted.

Simplified LS estimator using CCE-BEM Although we have investigated an efficient implementation above, it still has a fairly high complexity and thus one may hope to further simplify it. Among various (windowed) BEM’s, we observe that the basis functions of the CCE-BEM yield shifted identity matrices, i.e., $\mathbf{D}_q = \mathbf{F} \text{diag}\{\mathbf{q}_q\} \mathbf{F}^H = \mathbf{I}^{(q)}$ according to (6) since $\mathbf{q}_q = [1, e^{j\frac{2\pi}{N}q}, \dots, e^{j\frac{2\pi(N-1)}{N}q}]^T$ for the CCE-BEM; and $\mathbf{I}^{(q)}$ only contains 1’s on the q th (sub- or super-) diagonal but 0’s

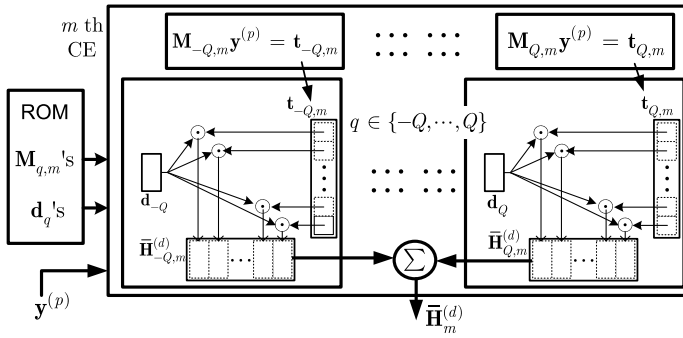
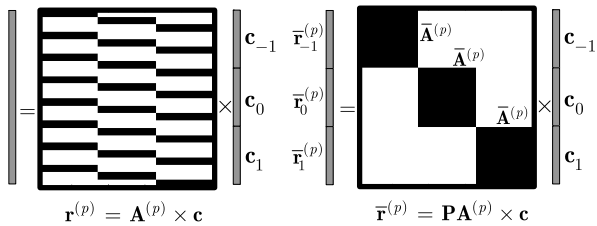


Fig. 4 Schematic of the m th general LS estimator

Fig. 5 Special matrix structure with CCE-BEM, where $Q = 1$ and $N_P = 8$ for instance, and \mathbf{P} is a permutation matrix



otherwise, and $\mathbf{I}^{(0)} = \mathbf{I}_N$ is an identity matrix. It also yields $\Theta \odot \mathbf{D}_{q,m}^{(d)} = \mathbf{D}_{q,m}^{(d)}$ in (17).

If we exploit this property (i.e., $\mathbf{D}_q = \mathbf{I}^{(q)}$) in (10), $\mathbf{A}^{(p)}$ is then yielded with the special sparse structure as shown in the left part of Fig. 5, where the blank area stands for zero entries. Moreover, if we introduce a permutation matrix \mathbf{P} which only contains 1's in the positions

$$\{(i + 1, \lfloor i/N_P \rfloor + (2Q + 1)i_{\text{mod}/N_P} + 1)\}_{i=0}^{N_P-1}$$

but 0's elsewhere, then since

$$\mathbf{P}\mathbf{D}^{(p)} = \mathbf{I}_{(2Q+1)N_P},$$

we obtain [cf. (10)]

$$\mathbf{P}\mathbf{A}^{(p)} = \mathbf{I}_{2Q+1} \otimes (\text{diag}(\mathbf{b}^{(p)})\mathbf{F}^{(L,p)})$$

is a block diagonal matrix as shown in the right part of Fig. 5 with every sub-block at the diagonal of $\mathbf{P}\mathbf{A}^{(p)}$ being the same submatrix given by

$$\bar{\mathbf{A}}^{(p)} = \text{diag}(\mathbf{b}^{(p)})\mathbf{F}^{(L,p)}.$$

Consequently, denoting $\bar{\mathbf{r}}^{(p)} = \mathbf{P}\mathbf{r}^{(p)} = [\bar{\mathbf{r}}_{-Q}^{(p)T}, \dots, \bar{\mathbf{r}}_Q^{(p)T}]^T$, we can split (11) in parallel for $q \in \{-Q, \dots, Q\}$ into

$$\hat{\mathbf{c}}_q = (\bar{\mathbf{A}}^{(p)H} \bar{\mathbf{A}}^{(p)})^{-1} \bar{\mathbf{A}}^{(p)H} \bar{\mathbf{r}}_q^{(p)}. \tag{21}$$

Note that the permutation operation by \mathbf{P} does not cost additional resources or processing latency, since it only refers to different access addresses into the memories in the hardware design.

Further observations based on $\mathbf{D}_q = \mathbf{I}^{(q)}$ suggest that the multiplication between $\Theta \odot \mathbf{D}_{q,m}^{(d)} = \mathbf{D}_{q,m}^{(d)}$ and $\text{diag}(\mathbf{F}_m^{(L,d)} \hat{\mathbf{c}}_q)$ in (17) only acts as placing the vector $\mathbf{F}_m^{(L,d)} \hat{\mathbf{c}}_q$ onto the $(Q + q)$ th diagonal line of the Toeplitz-like matrix $\hat{\mathbf{H}}_m^{(d)}$, for $q \in \{-Q, \dots, Q\}$. Let us use Fig. 3 for an illustration. When the CCE-BEM is used, the entries within the framed diagonal line in $\hat{\mathbf{H}}_m^{(d)}$ in Fig. 3 is actually equal to $\mathbf{F}_m^{(L,d)} \hat{\mathbf{c}}_q$ with $q = -1$. It is equivalent to say that in its DIA format $\bar{\mathbf{H}}_m^{(d)}$, the corresponding row $\bar{\mathbf{h}}_{q,m}^{(d)T}$ is actually composed by $\mathbf{F}_m^{(L,d)} \hat{\mathbf{c}}_q$, i.e., $\bar{\mathbf{h}}_{q,m}^{(d)} = \mathbf{F}_m^{(L,d)} \hat{\mathbf{c}}_q$. Therefore, if we jointly consider the fact that the estimator will yield a DIA format $\tilde{\mathbf{H}}_m^{(d)}$ instead of $\hat{\mathbf{H}}_m^{(d)}$, the operation in (17) acts equally as placing $\mathbf{F}_{L,m}^{(d)} \hat{\mathbf{h}}_q$'s onto the corresponding rows in $\bar{\mathbf{H}}_m^{(d)}$, for $q = \{-Q, \dots, Q\}$, when the CCE-BEM is used.

Now, we are allowed to describe the LS estimation tailored to the CCE-BEM, for $q \in \{-Q, \dots, Q\}$ and $m \in \{0, \dots, N_B - 1\}$, as

$$\bar{\mathbf{h}}_{q,m}^{(d)T} = \mathbf{F}_m^{(L,d)} \hat{\mathbf{c}}_q \tag{22}$$

and then, by substituting (21) into (22), we obtain

$$\bar{\mathbf{h}}_{q,m}^{(d)T} = \bar{\mathbf{M}}_m \bar{\mathbf{r}}_q^{(p)}, \tag{23}$$

where the $B \times N_P$ matrix $\bar{\mathbf{M}}_m$ is given by

$$\bar{\mathbf{M}}_m = \mathbf{F}_m^{(L,d)} (\bar{\mathbf{A}}^{(p)H} \bar{\mathbf{A}}^{(p)})^{-1} \bar{\mathbf{A}}^{(p)H}$$

which is also perfectly known at the receiver.

Finally, the yielded DIA format of each $\hat{\mathbf{H}}_m^{(d)}$ is stacked as

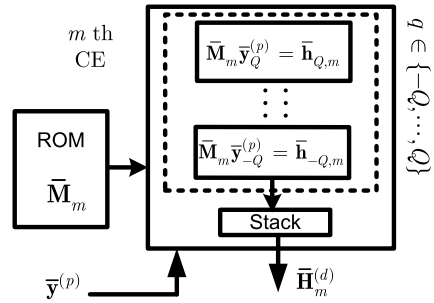
$$\tilde{\mathbf{H}}_m^{(d)} = [\bar{\mathbf{h}}_{-Q,m}^{(d)}, \dots, \bar{\mathbf{h}}_{Q,m}^{(d)}]^T.$$

We call this implementation method as the ‘‘Simplified LS Estimator’’, which is particularly tailored for the CCE-BEM. Its detailed implementation is described as Algorithm 2. Its computational complexity is listed in Table 1 for comparison with the previous method. It is clear that this simplified LS estimator is more economic and memory efficient than the previous general LS estimator. The schematic of the

Algorithm 2 Simplified LS estimator (for CCE-BEM)

0. Pre-compute the matrix all $\bar{\mathbf{M}}_m$'s for $m = \{0, \dots, N_B - 1\}$; Totally $N_D N_P$ elements are stored for ROM;
 1. Carefully collect $\bar{\mathbf{r}}_q^{(p)}$'s and perform (23) to attain $\bar{\mathbf{h}}_{q,m}^{(d)}$ for $q = \{-Q, \dots, Q\}$, which is stacked into a $(2Q + 1) \times B$ matrix $\tilde{\mathbf{H}}_m^{(d)}$, the DIA format of $\hat{\mathbf{H}}_m^{(d)}$.
-

Fig. 6 Schematic of the m th simplified LS estimator



simplified LS estimator is depicted in Fig. 6. To maximize the concurrency, the processing parallelism for both $q \in \{-Q, \dots, Q\}$ and $m \in \{0, \dots, N_B - 1\}$ can be exploited. It is noteworthy that, when $Q = 0$, (23) degrades to the channel estimation for the traditional OFDM systems which operate in the time-invariant channels. In other words, our simplified estimator tailored for the CCE-BEM can be considered as an extension of the channel estimator design for the time-invariant OFDM systems. One may argue that the CCE-BEM is inferior to other BEM models [21, 27] in terms of the modeling accuracy. We shall show that the CCE-BEM still yields a good performance of channel estimation in the presence of a realistic mobility velocity.

4.2 Channel Equalizer

To recover the m th data cluster denoted by a $B \times 1$ vector $\mathbf{b}_m^{(d)}$, a ZF equalization is introduced in (16), where a matrix inversion is required. For a traditional OFDM over a time-invariant channel, $Q = 0$ is efficient and thus $\hat{\mathbf{H}}_m^{(d)}$ is a diagonal matrix. In this case, the equalization (16) has only a computational complexity linear to the vector size B . However, when the channel is time varying, $\hat{\mathbf{H}}_m^{(d)}$ is in principle a full matrix, and thus the equalization complexity using its direct matrix inversion is too high (i.e., $\mathcal{O}(B^3)$ [9]) to be practical. An important feature is that each $\hat{\mathbf{H}}_m^{(d)}$ is a banded matrix with a bandwidth of $2Q + 1$ [cf. (18)], and thus $\hat{\mathbf{H}}_m^{(d)H} \hat{\mathbf{H}}_m^{(d)}$ is a banded positive definite Hermitian matrix. Based on this property, we can adapt the LDL^H factorization [9] to realize the inversion more efficiently, yielding a low-complexity equalization as specified in Algorithm 3. This equalization has a computational complexity $\mathcal{O}(Q^2 B)$, which is usually much less than $\mathcal{O}(B^3)$ because Q is typically small (e.g., $Q = 1$) [16]. Note that the above algorithm requires a strictly banded matrix $\hat{\mathbf{H}}_m^{(d)}$ [16], which also explains Θ in (17). We also need to note that the above process is correct, for $m = \{0, \dots, N_B - 1\}$, only if the number of null subcarriers at either edge is larger than the half bandwidth of $\hat{\mathbf{H}}_m^{(d)}$, i.e., $\geq Q$ [cf. Fig. 2]. Such a condition is widely considered in the literature in, e.g., [6, 7, 16, 17], and it can be satisfied in many existing OFDM standards, e.g., a multiple-band UWB standard. Table 2 specifies the complexity of the equalizer for the m th data cluster in complex operations, i.e. CAs, CMs, and complex dividers (CDs). In the same table, we also quote the complexity of our channel estimator tailored for the CCE-BEM from Table 1.

To implement the channel equalizer efficiently, we first recall that the DIA format $\bar{\mathbf{H}}_m^{(d)}$ is obtained by the channel estimator as described in the previous section, instead

Algorithm 3 Low-complexity equalization algorithm

1. Compute the matrix $\mathbf{W}_m = \hat{\mathbf{H}}_m^{(d)H} \hat{\mathbf{H}}_m^{(d)}$ and also $\mathbf{p} = \hat{\mathbf{H}}_m^{(d)H} \mathbf{r}_m^{(d)}$;
2. Perform the banded-LDL^H factorization as $\mathbf{W}_m = \mathbf{LDL}^H$, where \mathbf{D} is a diagonal matrix, and \mathbf{L} is a lower triangular matrix whose diagonal are ones and whose lower bandwidth is $2Q$; Such LDL^H factorization can be implemented in pseudo-code as:

```

D[0, 0] = Wm[0, 0];
for(i = 1; i < B; i = i + 1)
    u = max(0, i - 2Q);
    for(j = u; j < i; j = j + 1)
        L[i, j] =  $\frac{1}{\mathbf{D}[j, j]} (\mathbf{W}_m[i, j] - \sum_{k=u}^{j-1} \mathbf{L}^*[j, k] \mathbf{L}[i, k] \mathbf{D}[k, k]);$ 
    end
    D[i, i] =  $\mathbf{W}_m[i, i] - \sum_{k=u}^{i-1} |\mathbf{L}[i, k]|^2 \mathbf{D}[k, k];$ 
end
    
```

3. Solve $\mathbf{W}_m \hat{\mathbf{b}}_m^{(d)} = \mathbf{p}$ by solving firstly the triangular system $\mathbf{L}\mathbf{f} = \mathbf{p}$ and the diagonal system $\mathbf{D}\mathbf{g} = \mathbf{f}$, and then another triangular system $\mathbf{L}^H \hat{\mathbf{b}}_m^{(d)} = \mathbf{g}$ to recover $\hat{\mathbf{b}}_m^{(d)}$. This step can be specified in pseudo-code as

```

for(i = 0; i < B; i = i + 1)
    u = max(0, i - 2Q);
    f[i] =  $\mathbf{p}[i] - \sum_{k=u}^{i-1} \mathbf{L}[i, k] \mathbf{f}[k];$  g[i] = f[i]/D[i, i];
end
for(i = B - 1; i ≥ 0; i = i - 1)
    v = min(B - 1, i + 2Q);
     $\hat{\mathbf{b}}_m^{(d)}[i] = \mathbf{g}[i] - \sum_{k=i+1}^v \mathbf{L}^*[k, i] \hat{\mathbf{b}}_m^{(d)}[k];$ 
end
    
```

Table 2 Complexity analysis for the estimator and equalizer

Complex operations	Mobile OFDM		TI OFDM	
	Simplified CE	EQ	CE	EQ
CMs	$(2Q + 1)N_p B$	$(4Q^2 + 12Q + 2)B$	$N_p B$	0
CAs	$(2Q + 1)(N_p - 1)B$	$(4Q^2 + 8Q + 3)B$	$(N_p - 1)B$	0
CDs	0	$(2Q + 1)B$	0	<i>B</i>

of its original matrix $\hat{\mathbf{H}}_m^{(d)}$. Here, prior to the equalizer implementation, we describe how to efficiently store the matrices used in Algorithm 3 (i.e., $\mathbf{W}_m = \hat{\mathbf{H}}_m^{(d)H} \hat{\mathbf{H}}_m^{(d)}$, while \mathbf{L} and \mathbf{D} are obtained from $\mathbf{W}_m = \mathbf{LDL}^H$). Due to the special structures of these matrices, the DIA format is adapted herein. We plot Fig. 7 to illustrate the storage of these matrices, where $\bar{\mathbf{W}}_m$ is the adapted DIA format to store \mathbf{W}_m , while

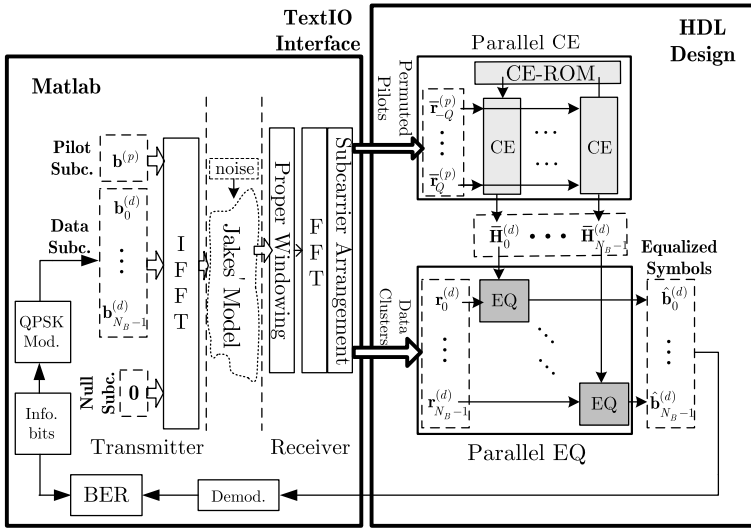


Fig. 10 Testbench of mobile OFDM baseband receiver

Table 3 Testing setups for OFDM system

Setup	Q	N	N_P	N_B	B	N_D	Edge Guard ^a
O	0	256	8	7	35	245	2
I	1	256	8	7	30	210	3
II	2	256	8	7	25	175	5
III	3	256	8	7	20	140	6

^aReferring to the edge null subcarriers. The number of the null subcarrier at either edge must be larger than Q . For simplicity reasons, we never place separated data subcarriers but only place them as N_B clusters, and thus abundant edge null subcarriers may exist

that the aforementioned channel estimator shares the same interfaces to communicate with our channel equalizer herein. Figure 10 describes the parallel connection between each pair of channel estimator (CE) and equalizer (EQ), and also illustrates the testbench environment used in this paper.

5 Experiments

For the OFDM setup, we consider the cases listed in Table 3. It is known that using a larger Q , a higher system performance with regards to the symbol detection accuracy can be obtained [6, 7, 16, 17, 21]. But its paid price is a higher hardware cost for implementation, which is evident later. Each pilot is guarded by $2Q$ null subcarriers on its either side. In addition to these guarded null subcarriers, the number of the null edge subcarriers placed at either edge is needed to be larger than Q . For all the cases,

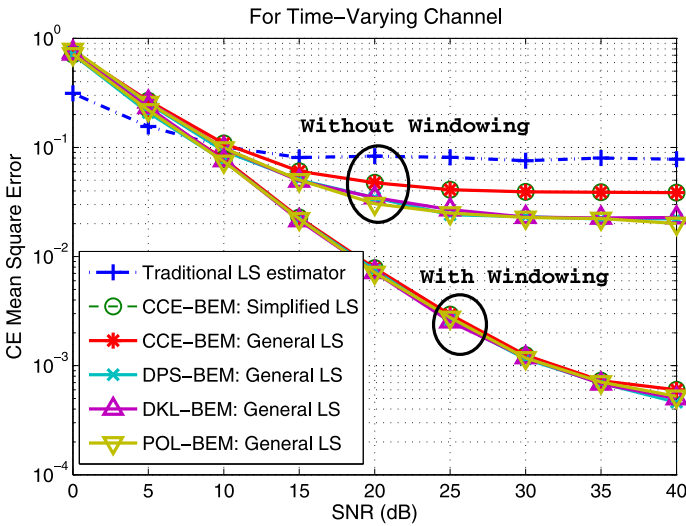


Fig. 11 Channel estimation accuracy

QPSK symbols are modulated on the data and pilot subcarriers; To represent the time-varying channels, the Jakes’ model [12] with a maximal normalized Doppler factor (i.e., the Doppler shift divided by the OFDM subcarrier interval) of 0.02 is adopted. Physically, if we consider that the OFDM baseband bandwidth is $W = 20$ MHz and the central radio frequency is $f_c = 10$ GHz, this maximal normalized Doppler factor corresponds to the highest velocity of $v = 84.38$ km/h (computed by $\frac{f_c \times 2v/c}{W/N} = 0.02$, where $c = 1.08 \times 10^9$ km/h). Moreover, the delay tap number of the channel is taken less than N_p , which means a delay spread of 0.4ms if the baseband bandwidth of $W = 20$ MHz, such that $N_p > L$ is satisfied [cf. (11)]. The time-varying channel is windowed by a time-domain windowing from [17]. According to the testbench environment as illustrated in Fig. 10, we randomly generate the received OFDM symbols for our LS channel estimator and ZF equalizer, and then examine the performances of the channel estimation and equalization.

Let us currently focus on the Setup O and Setup I for the OFDM system. Fig- ure 11 illustrates the mean-square-error (MSE) performances of the LS channel estimator using various BEM’s for the Setup I, with different signal-to-noise ratio (SNR) conditions. The traditional LS estimator for the time-invariant (TI) OFDM channels is realized using our simplified LS estimator corresponding to $Q = 0$ as previously mentioned. The MSE is defined as

$$\text{MSE} = \frac{1}{N_B} \sum_{m=0}^{N_B-1} \|\mathbf{H}_{F,m}^{(d)} - \hat{\mathbf{H}}_m^{(d)}\|^2 / \|\mathbf{H}_{F,m}^{(d)}\|^2, \tag{24}$$

where $\mathbf{H}_{F,m}^{(d)}$ is carved from \mathbf{H}_F in (1) at the same positions corresponding to $\hat{\mathbf{H}}_m^{(d)}$ in $\hat{\mathbf{H}}_F$. From Fig. 11, it is clear that the traditional estimator designed for TI channels cannot combat a time-varying channel, while the performances of our LS estimators

Table 4 Synthesis results of channel estimator

Method	ASIC Core Area ^a (10 ³ μm ²)	ROM Area ^a (10 ³ μm ²)	Latency ^a (cycle)
Simplified CE	487.46	25.24	159
General CE	1129.84	213.36	353

^a90 nm ASIC technology with 100 MHz clock and 20 (40) bits are adopted for a real (complex) number; Here $Q = 1$

without a time windowing are still not good. With a proper windowing design, our LS estimators all perform well for time-varying channels, no matter which BEM is adopted. It is noteworthy that although the estimation accuracy of a simplified LS estimator using the CCE-BEM is indeed inferior to other BEM models, the drop of the estimation accuracy is slight especially in presence of the time-domain windowing. Additionally, it is certain that the estimation accuracies obtained by using different implementation methods (i.e., general LS estimator or simplified LS estimator) are identical when the CCE-BEM is adopted to model the channel. In addition to BEM's, a Gauss–Markov process [5] can also be adopted to model time-varying channels. However, the Gauss–Markov process is mainly adopted for time-domain sequential processing [21], while in this paper we shall focus on the BEM which is often more convenient for block transmission schemes such as OFDM.

At the same time, we compare the hardware resource utilizations of the aforementioned two approaches of implementing the channel estimation (i.e., general LS estimator and simplified LS estimator). Setup I is tested. Specifically, using a similar methodology as [19], we first realize an LS estimator for one data cluster (e.g., the m th data cluster), and then duplicate it to generate other pairs with $Q = 1$, resulting a concurrency for $m = \{0, \dots, N_B - 1\}$. Table 4 lists the values of their synthesis results in a 90 nm technology. It shows that our simplified LS estimator brings a roughly 57 % cut for the ASIC core area (excluding the ROM), a 88 % savage for the ROM size and a 55 % reduction of the processing latency compared to the general LS estimator. Jointly considering their estimation performances shown in Fig. 11 and their hardware costs herein, it suggests that the it is more appealing to design time-varying OFDM systems using the CCE-BEM than using other BEM options.

Now, we select the simplified LS estimator tailored to the CCE-BEM and then combine it with the ZF channel equalizer. Figure 12 compares the bit-error ratio (BER) performance of our design using OFDM Setup I, II and III (i.e., with $Q = 1, 2$ and 3) for a narrowband time-varying channel. Additionally, we also build a TI OFDM receiver corresponds to OFDM Setup O using $Q = 0$ and without any time-domain windowing. We note that these BER performances are obtained without any channel coding. It is clear that since the TI OFDM receiver fails to combat the time variation of the channel, it hardly recover the transmitted data information correctly. However, the receiver using our estimator and equalizer significantly improves the BER performance especially at a higher SNR. In addition, the use of a larger Q parameter indeed brings a performance improvement with regards to the symbol detection accuracy, as noticed by [6, 7, 16, 17].

To investigate the hardware resource utilization of our designs, we implement the designs with these setups (i.e., with $Q = 0, 1, 2$ and 3). Similar for the channel estimator, we first realize a ZF equalizer in combination with a simplified LS estimator,

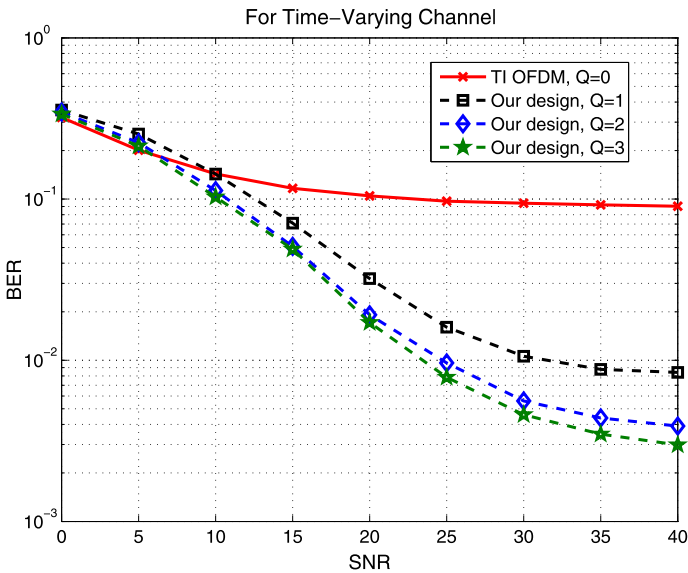


Fig. 12 BER performance

and then duplicate their combination for $m = \{0, \dots, N_B - 1\}$. Their synthesis results on a Xilinx 6VLX240TFF1156 device are listed in Table 5, where the processing latency is counted by the clock cycles and the FPGA resource utilization report is quoted. It is no surprise that a time-varying OFDM receiver (or a mobile OFDM receiver) based on the BEM requires more hardware efforts to support high-mobility users since we remarkably extend a TI OFDM system. In other words, the BER improvement of time-varying OFDM systems is earned at the price of more complicated hardware design, compared to a TI OFDM receiver. Moreover, we observe that for the time-varying OFDM system from $Q = 1$ to $Q = 3$, the hardware resource utilization (e.g., by considering “acc. Inst.” as an overall utilization of hardware resource), as well as the processing latency, increases roughly linearly along Q . Jointly considering the BER performance as illustrated in Fig. 12, an excessively large Q (e.g., $Q = 3$) is not desirable since a remarkable increased hardware cost only brings a slight improvement of the BER performance. For instance, a roughly 0.1dB BER improvement from $Q = 2$ to $Q = 3$ is obtained, but at a price of 1.32 times resource utilization. It indicates that a small Q is sufficient (e.g., $Q = 2$) to provide an accurate symbol detection without introducing too high hardware utilization.

6 Summary

The narrowband OFDM system model in light of BEM was introduced. Two efficient implementations for the least-squares estimator of OFDM time-varying channels were discussed. The first one is the general estimator which supports estimation methods using various BEM models. The second one, the simplified estimator

Table 5 Comparison of FPGA implementations

		Mobile OFDM			TI OFDM
		$Q = 3$	$Q = 2$	$Q = 1$	$Q = 0$
Latency (cycle)		2759	2451	1758	706
Resource ^a	acc. Inst.	128720	96966	69808	20163
	LUTs	40.02 %	35.69 %	27.14 %	6.88 %
	CLBs	40.05 %	35.71 %	27.18 %	6.94 %
	DFFs	3.70 %	3.22 %	2.32 %	0.98 %
	DSP48Es	28.52 %	25.43 %	18.24 %	4.16 %
	RAMS	65.77 %	58.73 %	42.25 %	8.94 %

^a20 (40) bits for a real (complex) number on Xilinx 6VLX240TFF1156 Device with a 100MHz clock; The RAMS stands for the block RAM components, which are mainly used to store matrices during the channel estimation and equalization

particularly tailored for the CCE-BEM, leads to a more efficient hardware architecture, while still maintains a high estimation accuracy. Hence, the CCE-BEM is more appealing to time-varying OFDM systems than other BEM's. The efficient implementation of the parallel equalizer was presented afterwards. Our design for OFDM receivers with a small BEM order is capable of combatting the narrowband time-varying OFDM channel. For comparison, a traditional time-invariant OFDM receiver design which only works for time-invariant channels fails in a time-varying channel.

Acknowledgements This work was supported in part by NSFC (project 61302140).

Appendix: Detailed Derivation of (9)

Let us start from the noiseless version of (8) as

$$\mathbf{r}^{(p)} = \sum_{q=-Q}^Q \mathbf{D}_q^{(p)} \Delta_q^{(p)} \mathbf{b}^{(p)},$$

where $\mathbf{D}_q^{(p)}$ is a submatrix obtained from \mathbf{D}_q by only selecting rows (columns) corresponding to $\mathbf{r}^{(p)}$ in \mathbf{r}_F ($\mathbf{b}^{(p)}$ in \mathbf{b}), and $\Delta_q^{(p)}$ is obtained from Δ_q by selecting the rows of $\mathbf{b}^{(p)}$ in \mathbf{b} .

We first notice that $\Delta_q = \text{diag}(\mathbf{F}^{(L)} \mathbf{c}_q)$ as specified in (7), and thus we can specify $\Delta_q^{(p)}$ as

$$\Delta_q^{(p)} = \text{diag}(\mathbf{F}^{(L,p)} \mathbf{c}_q),$$

where $\mathbf{F}^{(L,p)}$ collects the rows of $\mathbf{F}^{(L)}$ corresponding to the positions of $\mathbf{b}^{(p)}$ in \mathbf{b} .

To this end, it is clear that

$$\begin{aligned}\Delta_q^{(p)} \mathbf{b}^{(p)} &= \text{diag}(\mathbf{F}^{(L,p)} \mathbf{c}_q) \mathbf{b}^{(p)} \\ &= \text{diag}(\mathbf{b}^{(p)}) \mathbf{F}^{(L,p)} \mathbf{c}_q.\end{aligned}\quad (25)$$

Substituting (25) into $\mathbf{r}^{(p)}$, we obtain

$$\begin{aligned}\mathbf{r}^{(p)} &= \sum_{q=-Q}^Q \mathbf{D}_q^{(p)} (\text{diag}(\mathbf{b}^{(p)}) \mathbf{F}^{(L,p)}) \mathbf{c}_q \\ &= [\mathbf{D}_{-Q}^{(p)}, \dots, \mathbf{D}_Q^{(p)}] \\ &\quad \times \mathbf{I}_{2Q+1} \otimes (\text{diag}(\mathbf{b}^{(p)}) \mathbf{F}^{(L,p)}) \\ &\quad \times [\mathbf{c}_{-Q}^T, \dots, \mathbf{c}_Q^T]^T \\ &= \mathbf{D}^{(p)} (\mathbf{I}_{2Q+1} \otimes (\text{diag}(\mathbf{b}^{(p)}) \mathbf{F}^{(L,p)})) \mathbf{c},\end{aligned}\quad (26)$$

where \otimes stands for the Kronecker product, $\mathbf{D}^{(p)} = [\mathbf{D}_{-Q}^{(p)}, \dots, \mathbf{D}_Q^{(p)}]$ and $\mathbf{c} = [\mathbf{c}_{-Q}^T, \dots, \mathbf{c}_Q^T]^T$.

Consequently, if we denote

$$\mathbf{A}^{(p)} = \mathbf{D}^{(p)} (\mathbf{I}_{2Q+1} \otimes (\text{diag}(\mathbf{b}^{(p)}) \mathbf{F}^{(L,p)}))$$

as defined in (10), we obtain

$$\mathbf{r}^{(p)} = \mathbf{A}^{(p)} \mathbf{c}$$

which is the noiseless version of (9).

References

1. J.A.C. Bingham, Multicarrier modulation for data transmission: an idea whose time has come. *IEEE Commun. Mag.* **28**, 5–14 (1990)
2. D.K. Borah, B.D. Hart, Frequency-selective fading channel estimation with a polynomial time-varying channel model. *IEEE Trans. Commun.* **47**, 862–873 (1999)
3. X. Cai, G.B. Giannakis, Bounding performance and suppressing intercarrier interference in wireless mobile OFDM. *IEEE Trans. Commun.* **51**, 2047–2056 (2003)
4. C. Dick, F. Harris, FPGA implementation of an OFDM PHY, in *Proc. Asilomar Conference on Signals, Systems, and Computers*, vol. 1 (2003), pp. 905–909
5. M. Dong, L. Tong, B. Sadler, Optimal insertion of pilot symbols for transmissions over time-varying flat fading channels. *IEEE Trans. Signal Process.* **52**, 1403–1418 (2004)
6. K. Fang, G. Leus, L. Rugini, Block transmissions over doubly-selective channels: iterative channel estimation and turbo equalization. *EURASIP J. Adv. Signal Process.* **2010**, 13 (2010)
7. K. Fang, L. Rugini, G. Leus, Low-complexity block turbo equalization for OFDM systems in time-varying channels. *IEEE Trans. Signal Process.* **56**, 5555–5566 (2008)
8. G.B. Giannakis, C. Tepedelencioglu, Basis expansion models and diversity techniques for blind identification and equalization of time-varying channels. *Proc. IEEE* **86**, 1969–1986 (1998)
9. G.H. Golub, C.F. van Loan, *Matrix Computations*, 3rd edn. (Johns Hopkins Press, Baltimore, 1996)

10. T. Hrycak, S. Das, G. Matz, H.G. Feichtinger, Low complexity equalization for doubly selective channels modeled by a basis expansion. *IEEE Trans. Signal Process.* **58**, 5706–5719 (2010)
11. E.-J. Im, Optimizing the performance of sparse matrix-vector multiplication. Ph.D. thesis, University of California, Berkeley (2000)
12. W.C. Jakes, *Microwave Mobile Communications* (Wiley, New York, 1974)
13. G. Leus, On the estimation of rapidly time-varying channels, in *Proc. Europ. Signal Process. Conf., EUSIPCO*, Vienna, Austria (2004)
14. X. Ma, G.B. Giannakis, Maximum-diversity transmissions over doubly selective wireless channels. *IEEE Trans. Inf. Theory* **49**, 1832–1840 (2003)
15. X. Ma, G.B. Giannakis, S. Ohno, Optimal training for block transmissions over doubly selective wireless fading channels. *IEEE Trans. Signal Process.* **51**, 1351–1366 (2003)
16. L. Rugini, P. Banelli, G. Leus, Simple equalization of time-varying channels for OFDM. *IEEE Commun. Lett.* **9**, 619–621 (2005)
17. L. Rugini, P. Banelli, G. Leus, Low-complexity banded equalizers for OFDM systems in doppler spread channels. *EURASIP J. Appl. Signal Process.* **2006**, 248 (2006)
18. P. Schniter, Low-complexity equalization of OFDM in doubly selective channels. *IEEE Trans. Signal Process.* **52**, 1002–1011 (2004)
19. A. Takach, B. Bowyer, T. Bollaert, C based hardware design for wireless applications, in *Proc. Design, Auto. and Test in Europe*, DATE (2005), pp. 124–129
20. Y. Tang, L. Qian, Y. Wang, Optimized software implementation of a full-rate IEEE 802.11a compliant digital baseband transmitter on a digital signal processor, in *Proc. IEEE Global Commun. Conf., GLOBECOM*, vol. 4, (2005)
21. Z. Tang, R.C. Cannizzaro, G. Leus, P. Banelli, Pilot-assisted time-varying channel estimation for OFDM systems. *IEEE Trans. Signal Process.* **55**, 2226–2238 (2007)
22. Z. Tang, G. Leus, Time-varying MIMO–OFDM channel estimation with aid of pilots. *EURASIP J. Adv. Signal Process.* **1**, 74 (2011)
23. Z. Tang, R. Remis, M.L. Nordenvaad, On preconditioned conjugate gradient method for time-varying OFDM channel equalization, in *Proc. IEEE Int. Conf. Acoust., Speech, Signal Process. (ICASSP)*, vol. 5 (Kyoto Press, Kyoto, 2012), pp. 2119–2122
24. S. Tomasin, A. Gorokhov, H. Yang, J.-P. Linnartz, Iterative interference cancellation and channel estimation for mobile OFDM. *IEEE Trans. Wirel. Commun.* **4**, 238–245 (2005)
25. M. Visintin, Karhunen–Loève expansion of a fast Rayleigh fading process. *IET Electron. Lett.* **32**, 1712–1713 (1996)
26. Z. Wang, G.B. Giannakis, Wireless multicarrier communications: where Fourier meets Shannon. *IEEE Signal Process. Mag.* **17**, 29–48 (2000)
27. T. Zemen, C.F. Mecklenbrauker, Time-variant channel estimation using discrete prolate spheroidal sequences. *IEEE Trans. Signal Process.* **53**, 3597–3607 (2005)